https://doi.org/10.5194/egusphere-2025-5306
Preprint. Discussion started: 3 December 2025


# Arctic Sea Ice Loss Amplifies Local Evaporation Influence on Water Vapor Isotopes: Insights from Cruise Observations

Yuankun Zhang [1], Zhongfang Liu [1], Dongsheng Li [1], Zhiqing Li [1], Hebin Shao [2]

[1]State Key Laboratory of Marine Geology, Tongji University, Shanghai, 200000, China
[2]Key Laboratory for Polar Science of the MNR, Polar Research Institute of China, Shanghai 200136, China

*Correspondence to*: Zhongfang Liu (liuzf406@tongji.edu.cn)

**Abstract.** Rapid Arctic warming and sea ice retreat have increased atmospheric humidity, yet the relative contributions of local evaporation and advected lower-latitude moisture remain poorly quantified. Here, we present high-resolution, ship-based in-situ measurements of near-surface water vapor isotopes across diverse Arctic sea ice regimes. By integrating isotope fractionation models with multi-source meteorological data, we show that sea ice changes act as a key modulator of Arctic water vapor isotopic variations. Under ice-covered conditions, water vapor isotopes are controlled by Rayleigh distillation, producing depleted $\delta^{18}O$ with a strong temperature dependence and elevated d-excess from ice-phase processes. As sea ice retreats, kinetic fractionation from local evaporation becomes increasingly important, particularly at temperatures above ~5 °C, generating enriched $\delta^{18}O$, elevated d-excess, and a characteristic "anti-temperature" effect. A Bayesian isotope mixing model quantifies the resulting moisture source shift, showing local evaporation contributions rise from 9.3 % in ice-covered regions to 22.7 % in melt regions, despite advected moisture remaining predominant. These findings establish a process-based isotope framework for the Arctic hydrological cycle, complementing conventional meteorological diagnostics and offering a robust benchmark for interpreting paleo-isotope archives.

## 1 Introduction

Stable water vapor isotopes ($\delta^{18}O$ and $\delta D$) and their derived deuterium excess (d-excess, defined as $\delta D - 8\times\delta^{18}O$) are widely used as tracers for investigating hydrological processes and identifying moisture sources (Gat, 1996). These parameters vary during phase transitions such as evaporation, condensation, and sublimation, encoding information about environmental conditions both at the moisture source and along the atmospheric transport pathways (Dansgaard, 1964; Galewsky et al., 2016; Bowen et al., 2019). As such, analysis of these isotopic parameters in modern water vapor and paleoclimate archives provides key insights into moisture sources and climatic dynamics across both modern (Kurita, 2011; Kopec et al., 2016; Wang et al., 2023) and paleoclimate contexts (Klein and Welker, 2016; Opel et al., 2013; Porter et al., 2019). This dual perspective is particularly critical in the Arctic, which serves not only as a modern laboratory of rapid hydrological change but also as a primary archive of past climate preserved in its ice sheets.

Recent Arctic amplification and sea ice loss have moistened the Arctic atmosphere (Min et al., 2008; Bengtsson et al., 2011; Bintanja and Selten, 2014), yet the relative roles of local evaporation and poleward moisture transport remain contested. Some studies attribute these changes to enhanced local evaporation over newly ice-free ocean, while others emphasize strengthened

https://doi.org/10.5194/egusphere-2025-5306
Preprint. Discussion started: 3 December 2025


poleward transport of lower-latitude moisture (Graversen et al., 2008; Screen et al., 2012; Kopec et al., 2016; Ford and Frauenfeld, 2022). Resolving this debate is crucial because water vapor plays a central role in Arctic radiative and hydrological feedbacks, influencing cloud cover, precipitation, and surface warming. Stable water vapor isotopes provide a process-based diagnostic for disentangling and quantifying these source contributions. Such insights are essential not only for improving the representation of hydrological processes in climate models, thereby enabling more reliable projections (Barras and Simmonds, 2009; Gao et al., 2011; Sturm et al., 2010; Xi, 2014), but also for interpreting isotopic signals preserved in paleoclimate archives such as ice cores (Klein et al., 2016; Opel et al., 2013; Porter et al., 2019).

However, the application of stable isotopes in the Arctic remains challenging due to conflicting interpretations of isotopic signals, particularly regarding the role of local evaporation. One line of evidence associates high d-excess and low $\delta^{18}O$ over open water with strong evaporation under cold, dry air masses (Kurita, 2011; Steen-Larsen et al., 2013; Mellat et al., 2021; Bailey et al., 2021). In contrast, other studies argue that lower-latitude vapor, which is inherently enriched in d-excess, dominates poleward transport, while sea ice loss enriches $\delta^{18}O$ and suppresses d-excess through enhanced local evaporation (Kopec et al., 2016; Song et al., 2023; Klein et al., 2015). These divergent interpretations largely reflect the scarcity of spatially extensive, high-resolution vapor isotope observations across the Arctic Ocean. Most existing studies are based on land-based observations, with limited coverage over the Arctic Ocean, hindering efforts to disentangle complex isotope signals (Kurita, 2011; Kopec et al., 2016; Mellat et al., 2021). Klein and Welker (2016) suggested the relative influence of local evaporation on water vapor isotopes may vary with sea ice extent (SIE), proposing an anti-correlation between d-excess and SIE. However, subsequent studies have reported the opposite relationship (Bonne et al., 2019). This persistent inconsistency underscores the need for broader, in-situ water vapor isotope observations across diverse sea ice regimes.

To address this gap, we leverage a unique set of high-resolution, in-situ water vapor isotope measurements obtained during a comprehensive summer expedition across the Arctic Ocean aboard the RV *Xuelong 2*. This dataset provides extensive spatial coverage across the Arctic, spanning sea ice regimes from near-continuous cover to open water. By integrating these isotopic observations with meteorological data, and applying isotope-based diagnostics along with Lagrangian trajectory analysis, this study aims to: (1) map the spatial patterns of summer Arctic vapor isotopes in relation to diverse sea ice regimes, (2) identify the primary mechanisms behind isotope variability under distinct sea ice conditions, and (3) quantify the partitioning between locally evaporated and advected moisture sources across different Arctic regions.

## 2 Data and Methods

### 2.1 Water Vapor Isotope Measurements and Calibration

We conducted continuous, in situ measurements of near-surface water vapor isotopes and humidity at 1-second resolution during the 14th Chinese Arctic Research Expedition, using a Picarro L-2130i cavity ring-down spectroscopy (CRDS) analyzer deployed onboard the research vessel *Xuelong 2*. To ensure representative sampling of the marine boundary layer, ambient air was drawn from an inlet ~10 m above sea level and routed to the analyzer through a 5-meter inlet tube.

https://doi.org/10.5194/egusphere-2025-5306
Preprint. Discussion started: 3 December 2025


All isotope values are reported in standard δ notation relative to the Vienna Standard Mean Ocean Water (VSMOW):

$$\delta = \left(\frac{R_{sample}}{R_{VSMOW}} - 1\right) \times 1000 \quad (1)$$

where $R_{sample}$ and $R_{VSMOW}$ are the isotope ratios ($^{18}O/^{16}O$ or $^{2}H/^{1}H$) of the sample and VSMOW, respectively. The measurement precision was better than 0.04 ‰ for $\delta^{18}O$ and 0.5 ‰ for δ. D-excess was calculated following Dansgaard (1964) as:

$$d\text{-excess} = \delta D - 8 \times \delta^{18}O \quad (2)$$

Because the isotope measurements from the Picarro analyzer are subject to ambient water vapor concentration, a humidity-dependent correction was applied to ensure consistency across varying atmospheric conditions. Calibration was performed using a Standard Delivery Module (SDM). To define the calibration gradient, we used the analyzer's internal humidity measurements, which closely agree with independent sensors (Wang et al., 2023; Bonne et al., 2019), without relying on external references. Following Liu et al. (2014), two VSMOW-standard waters were analyzed at three humidity levels (5000, 15000, and 25000 ppm), each maintained for 20 minutes. A full calibration cycle was performed approximately every 22 hours during atmospheric measurements. To minimize memory effects, the first 10 minutes and final 2 minutes of each calibration step were excluded. A correction function was derived from the valid calibration data to express isotope bias as a function of humidity and was applied to all samples to normalize their values to a reference humidity of 20000 ppm:

$$\delta_{measured} - \delta_{humidity\ calibration} = f(humidity_{measured} - 20000) \quad (3)$$

All vapor isotope measurements were then normalized to the VSMOW scale using two standard waters ($\delta^{18}O$ = –11.018 ‰, δD = –78.051 ‰; $\delta^{18}O$ = –29.86 ‰, δD = –222.86 ‰), whose isotope values match the expected range of water vapor isotopes in the Arctic. Both standards were pre-corrected for humidity-dependent bias, and a linear calibration function was established based on the measured versus true values of the two standards and applied to all samples to complete the VSMOW normalization.

### 2.2 Meteorological and sea ice data

Meteorological data, including air temperature ($T$), relative humidity (RH), and air pressure, were obtained from the onboard weather station of the RV *Xuelong 2*. Specific humidity ($q$) was calculated from the water vapor concentration measured by the Picarro instrument. All datasets were synchronized to the isotope measurement timestamps (UTC+8) and averaged to 1-minute resolution. Surface evaporation flux ($E$), representing the instantaneous vertical water vapor flux from the ocean surface, was obtained from the fifth-generation European Centre for Medium-Range Weather Forecasts reanalysis (ERA5; Hersbach et al. (2023)), available at 1-hour temporal and 0.5° × 0.5° horizontal resolution.

The daily 4-km sea ice concentration (SIC) data were obtained from the National Snow and Ice Data Center (NSIDC), specifically from the MASIE-AMSR2 (MASAM2) blended product (Fetterer, 2023). This product integrates data from the

https://doi.org/10.5194/egusphere-2025-5306
Preprint. Discussion started: 3 December 2025


Multisensor Analyzed Sea Ice Extent (MASIE) and the Advanced Microwave Scanning Radiometer 2 (AMSR2). To assess the influences of sea ice on water vapor isotopes and moisture source partitioning, the Arctic was classified into three sea ice regimes using contemporaneous SIC data (Fig. 2):

I. Melt Region (SIC < 0.4): Areas below satellite detection threshold (MASAM-2 SIC = 0)

II. Sea Ice Region (SIC > 0.85): Predominantly ice-covered areas

III. Transition Region (0.4 ≤ SIC ≤ 0.85): Intermediate ice conditions

### 2.3 Theoretical Isotope Modelling of Ocean Evaporation

We employed the MJ79 model (Merlivat and Jouzel, 1979) to estimate the isotopic composition of water vapor evaporated from Arctic ocean, following the formulation of Bonne et al. (2019):

$$R_{BL} = \frac{R_{SW}}{\alpha_{eq} \times (\alpha_k + RH(1-\alpha_k))}, \quad (4)$$

where $R_{BL}$ is the isotopic ratio of water vapor in the boundary layer, and $R_{SW}$ is the isotopic ratio of surface seawater. RH is the relative humidity at the sea surface. $\alpha_{eq}$ and $\alpha_k$ are the equilibrium and kinetic fractionation coefficients, respectively. $\alpha_{eq}$ was calculated as a function of temperature, while $\alpha_k$ takes values of 1.0060 for $\delta^{18}O$ and1.0053 for $\delta D$ under smooth wind conditions, and 1.0035 for $\delta^{18}O$ and 1.0031 for $\delta D$ under rough wind conditions (Bonne et al., 2019). Because surface seawater isotope values in the open Arctic Ocean are typically close to 0 ‰ (Namyatov et al., 2024, 2023), we prescribed $\delta^{18}O$ and $\delta D$ of surface seawater as 0 ‰, from which $R_{SW}$ was calculated and used as the model input.

### 2.4 Back-trajectory calculation

To identify moisture sources in the Arctic, we analyzed air mass trajectories using the Hybrid Single Particle Lagrangian Integrated Trajectory (HYSPLIT) model (Stein et al., 2015). The model was driven by 0.5°×0.5° Global Data Assimilation System (GDAS) meteorological fields from the National Oceanic and Atmospheric Administration (NOAA) Air Resources Laboratory. Five-day backward trajectories were computed hourly from the cruise track at 10 m altitude, close to the height of the onboard weather station and Picarro inlet. This setting is consistent with the 4–5 day residence time of atmospheric water vapor and its concentration in the lower atmosphere (Gimeno et al., 2021; Wallace and Hobbs, 2006). All trajectories were batch-processed using the HYSPLIT Python package (Warner, 2018).

### 2.5 Bayesian isotope mixing model

To quantify the contributions of different moisture sources to Arctic water vapor, we employed MixSIAR (Stock and Semmens, 2016a), an open-source Bayesian mixing model implemented in R. MixSIAR, developed from earlier MIXSIR and SIAR, has been widely applied in ecological and environmental studies. According to Stock et al. (2018), the model framework can be expressed as:

https://doi.org/10.5194/egusphere-2025-5306
Preprint. Discussion started: 3 December 2025


$$Y_j = \sum_k p_k u_{jk}^s \ , \quad (5)$$

where $Y_j$ is the tracer value of the mixture for tracer $j$, $p_k$ is the proportional contribution of source k, and $u_{jk}^s$ is the mean tracer value of source $k$. Given the substantial isotopic variability in Arctic water sources and its propagation into the vapor mixture, we evaluated three error structures (residual, process, multiplicative) and adopted the process error structure as most appropriate (Stock and Semmens, 2016b):

$$Y_{ij} \sim N\left(\sum_k p_k u_{jk}^s , \sum_k p_k^2 \omega_{jk}^{s2}\right) \quad (6)$$

where $\omega$ represents the source variance of the two stable isotope tracers. MixSIAR then performed Markov Chain Monte Carlo (MCMC) sampling, estimating posterior probability distributions across all proportional source combinations.

## 3 Results

### 3.1 Water Vapor Isotope Variability Along the Cruise Track

Figure 1 shows the co-variation of near-surface water vapor isotopes and sea ice coverage along the trans-Arctic RV *Xuelong 2* expedition track spanning the Chukchi Sea, central Arctic Basin, Barents Sea, and Laptev–East Siberian Seas. $\delta^{18}O$ exhibited a pronounced spatial gradient along the cruise track, with the most enriched values (−10.8 ‰) in the ice-free Barents Sea, gradually becoming depleted poleward to the most depleted values (−34.19 ‰) in the heavily ice-covered central Arctic (SIC > 90 %), a pattern that inversely mirrors the gradient in sea ice coverage (Fig. 1a). This anti-phase variation between water vapor $\delta^{18}O$ and sea ice coverage is further confirmed by the $\delta^{18}O$ distributions across different sea-ice coverage regions (Fig. 2a), which reveal a systematic $\delta^{18}O$ enrichment from the Sea Ice Region (median = −23.97 ‰), through the Transition Region (−20.54 ‰), to the Melt Region (−18.83 ‰). These results suggest that sea ice changes can exert a strong influence on water vapor isotope composition of across the Arctic.

In contrast, the second-order parameter d-excess exhibits a more complex spatial pattern, with elevated values primarily observed both near coastal regions and in some localized zones of the ice-covered central basin (Fig. 1b). The highest values (23.31 ‰) were recorded in the central basin under steady sea ice cover, while the lowest (−8.35 ‰) occurred in the Chukchi Sea amid fluctuating sea ice (SIC varied from 40 % to 85 %). When grouped by SIC regimes, both the Melt and Sea Ice Regions sustained relatively higher d-excess values (median = 7.71 ‰ and 8.85 ‰, respectively), whereas the Transition Region yielded the lowest values (median = 5.46 ‰) (Fig. 2b). This distinct d-excess pattern across sea ice regimes points to the influence of sea ice changes on Arctic water vapor isotopic composition, likely through shifts in moisture sources and kinetic fractionation processes.

To examine how sea ice changes modulate Arctic water vapor isotopes, we show the variations of $\delta^{18}O$ and d-excess in relation to temperature, humidity, and local evaporation along the cruise track (Fig. 3). A comparison across the three sea ice regimes reveals that $\delta^{18}O$ and d-excess exhibited pronounced, anti-phase fluctuations (Fig. 3b). Depleted $\delta^{18}O$ generally coincided with

https://doi.org/10.5194/egusphere-2025-5306
Preprint. Discussion started: 3 December 2025


colder, drier air in the ice-covered central Arctic, while enriched values occurred in warm, moist sectors like the Barents Sea (Fig. 3d). The episodes of high d-excess were closely associated with conditions of reduced relative humidity and enhanced evaporation, particularly in the Melt Region (Fig. 3c), highlighting the growing role of kinetic fractionation under diminishing sea ice. These co-variations demonstrate that the sea ice regimes set the boundary conditions for the atmospheric controls—from equilibrium (temperature-driven) to kinetic (evaporation-driven)—on Arctic water vapor isotopes.

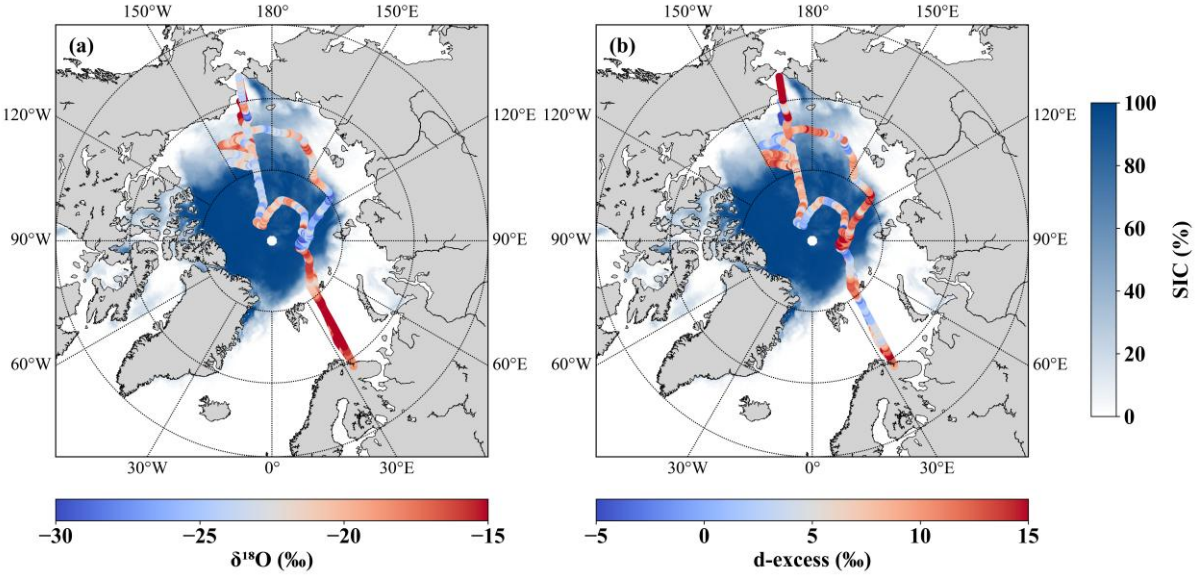


**Figure 1. Spatial distributions of water vapor δ¹⁸O (a) and d-excess (b) along the cruise track. Colored dots indicate measured isotopic values (‰) and shading shows the mean sea ice concentration (SIC) during the observation period.**

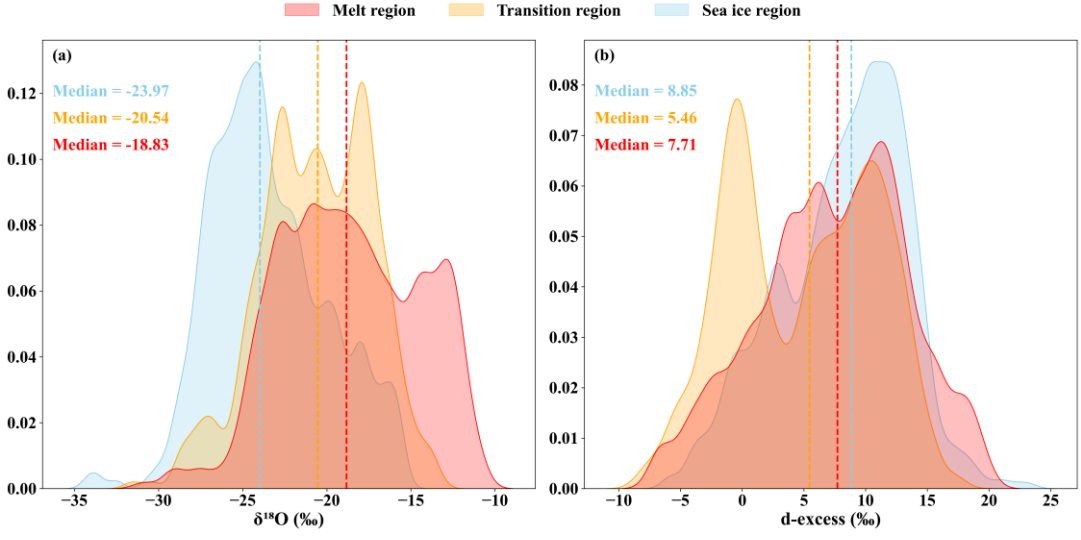


**Figure 2. Probability density distributions of δ¹⁸O (a) and d-excess (b) in the sea ice Melt (red), Transition (orange), and Sea Ice (blue) regions. Median values for each region are indicated.**

https://doi.org/10.5194/egusphere-2025-5306
Preprint. Discussion started: 3 December 2025


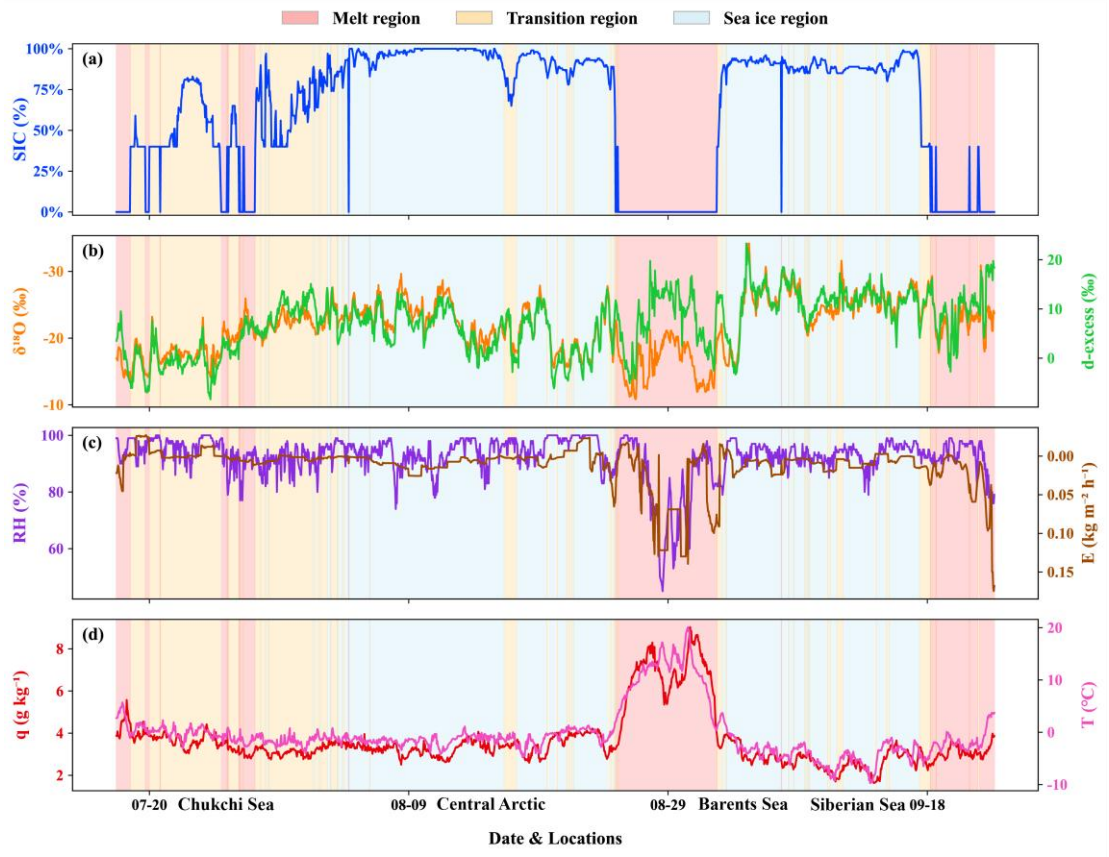


**Figure 3. Temporal and spatial evolution of observed water vapor isotopes, SIC, and meteorological parameters along the cruise routes. (a) SIC (%); (b) $\delta^{18}O$ (‰) and d-excess (‰); (c) Relative humidity (RH; %) and Evaporation (*E*; kg $m^{-2}$ $h^{-1}$); (d) Specific humidity (*q*; g $kg^{-1}$) and air temperature (*T*; °C). Background colors indicate the three different sea ice regimes.**

### 3.2 Isotopic Responses to Temperature and Humidity across Arctic Sea Ice Regimes

To investigate isotopic responses to temperature and humidity, we first examined the relationship between $\delta^{18}O$ and air temperature in the three distinct sea ice regions. As expected, $\delta^{18}O$ values exhibit significant positive correlations with temperature in all regions (Fig. 4a–c), consistent with the classical "temperature effect" (Dansgaard, 1964). However, this relationship weakens notably in the Melt Region and reverses when temperatures exceed 5 °C. Above this threshold, $\delta^{18}O$ becomes negatively correlated with temperature, indicating a departure from equilibrium-driven fractionation and the emergence of dominant kinetic processes under warm, ice-free conditions.

In contrast, d-excess shows a more variable response to temperature. Significant negative correlations are observed in the Sea Ice and Transition Regions ($r$ = –0.62 and –0.49, respectively; Fig. 4e, f), whereas the Melt Region exhibits a weak positive correlation ($r$ = 0.19; Fig. 4d). In the Melt Region, the correlation shifts from negative to positive when temperature is above 5 °C, highlighting a transition in the dominant fractionation regime. Although d-excess is theoretically not expected to directly depend on temperature (Shao et al., 2021; Xiang et al., 2022), previous studies have shown that a positive correlation can

https://doi.org/10.5194/egusphere-2025-5306
Preprint. Discussion started: 3 December 2025


emerge as a signature of oceanic evaporation (Uemura et al., 2008). This suggests that correlation between d-excess and temperature may serve as a diagnostic of the influence of local evaporation on Arctic water vapor (Brunello et al., 2023). Collectively, these patterns indicate that fractionation mechanisms undergo fundamental shifts as sea ice retreats, with kinetic effects increasingly dominating over open water.

Relative humidity (RH) further modulates isotopic fractionation by controlling the ambient saturation deficit (Bonne et al., 2019). Across all sea ice regimes, d-excess exhibits a consistent negative correlation with RH (Fig. 5a–c), with the strongest correlation in the Melt Region ($r = –0.52$, $p < 0.0001$), followed by the Transition ($r = –0.37$) and Sea Ice Regions ($r = –0.33$). A similar pattern is observed for the relationship between d-excess and surface evaporation (Fig. 5d–f), with the strongest positive correlation in the Melt Region ($r = 0.51$) and weaker ones in the Transition ($r = 0.40$) and Sea Ice ($r = 0.24$) Regions. These results indicate that as sea ice retreats, local evaporation increasingly governs the isotopic composition of Arctic water vapor, consistent with the elevated d-excess observed in ice-free areas, while its influence remains relatively weak in ice-covered regions.

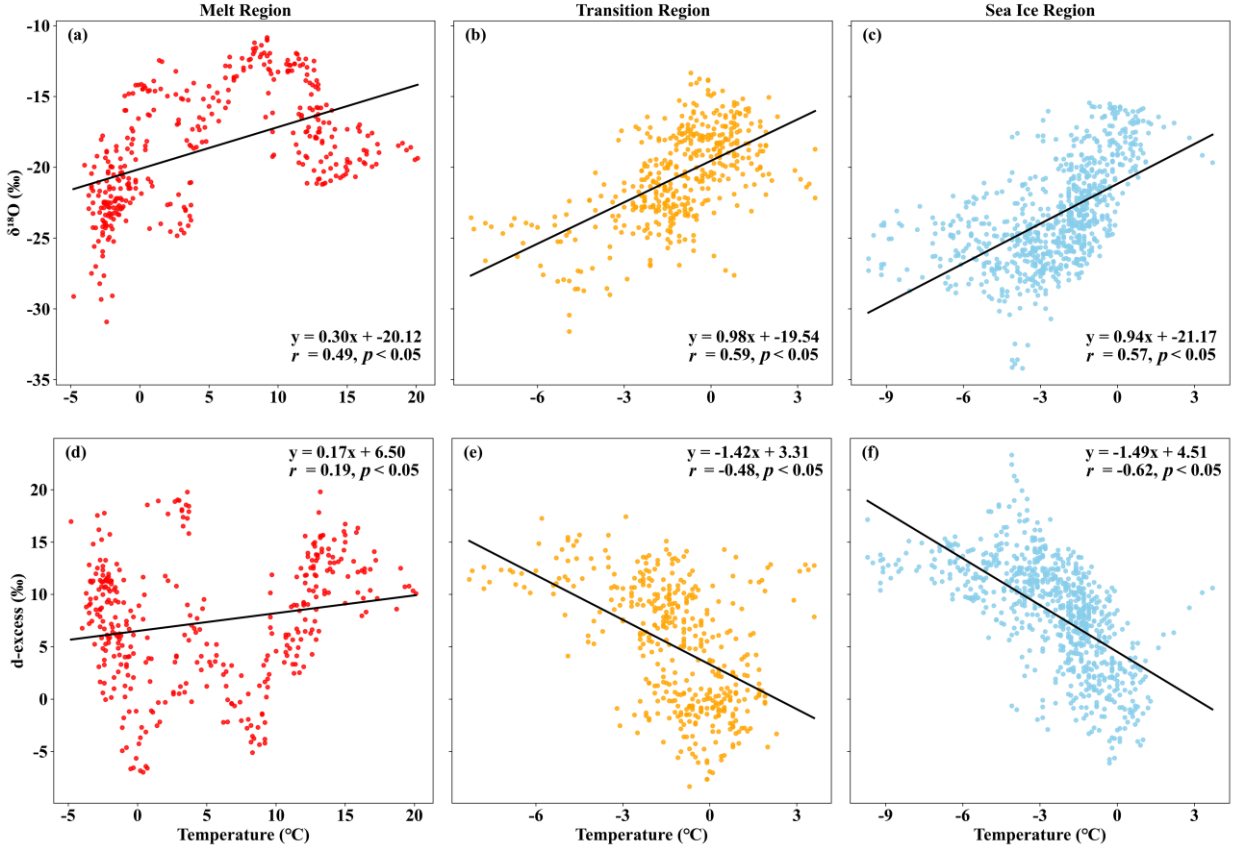


**Figure 4. (a-c) Relationships between $\delta^{18}O$ and air temperature across the three sea-ice regimes. (d-f) Same as (a-c) but for d-excess. Black lines denote linear regression fits.**

https://doi.org/10.5194/egusphere-2025-5306
Preprint. Discussion started: 3 December 2025


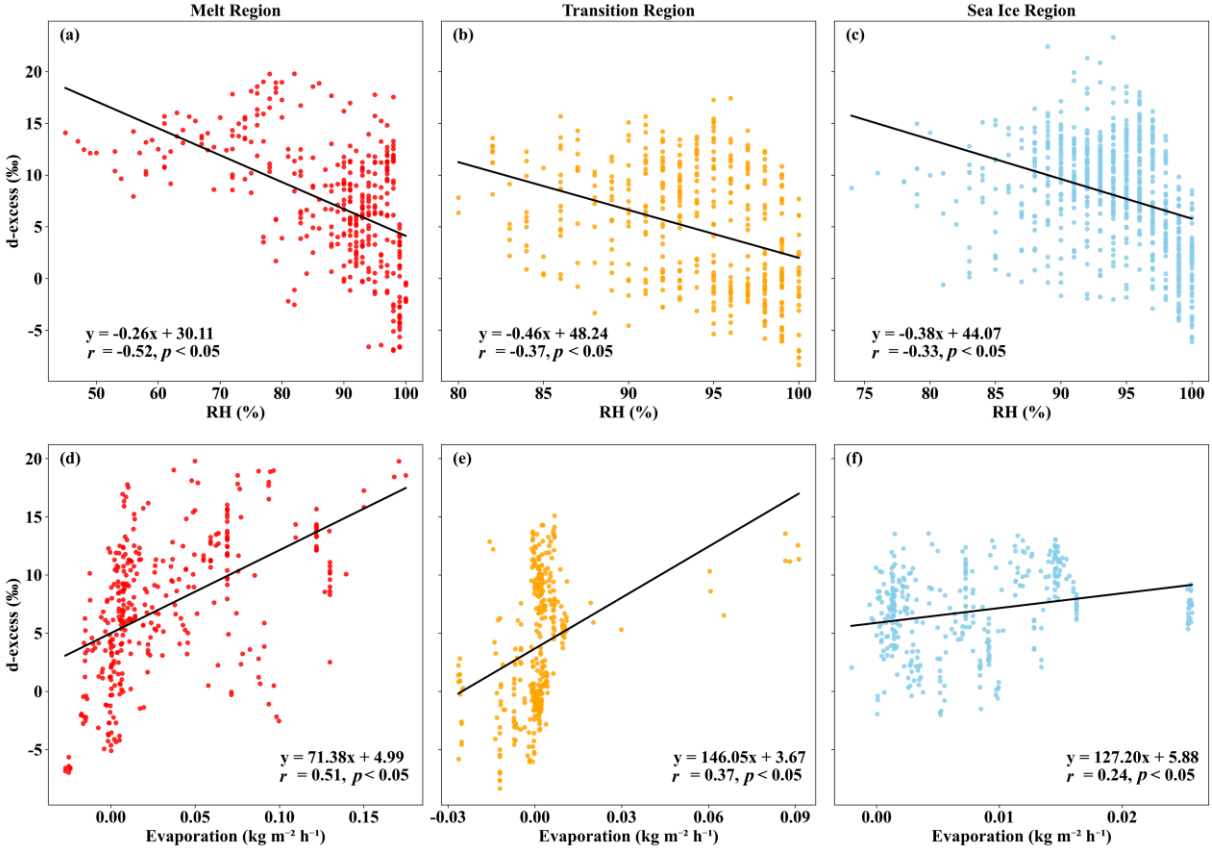


**Figure 5. (a-c) Relationships between d-excess and relative humidity (RH). (d-f) Relationships between d-excess and Evaporation. Black lines represent linear regression fits.**

### 3.3 Moisture Sources and Fractionation Processes across Arctic Sea Ice Regimes

To disentangle the influences of equilibrium and kinetic fractionation on Arctic water vapor isotopes, we employ *q*–δ diagrams as a diagnostic tool (Fig. 6a). Within a Rayleigh framework, $\delta^{18}O$ decreases systematically as vapor is progressively depleted through condensation during long-range transport, whereas d-excess remains relatively constant (Worden et al., 2007; Galewsky and Samuels-Crow, 2015; Noone, 2012). In the *q*–δ diagram, the idealized Rayleigh process forms a reference trajectory along which data distributions reflect the dominant influence of equilibrium fractionation. Data points deviating from this trajectory indicate additional physical processes: values above the curve often reflect admixture with other air masses (Wang et al., 2023), those below the mixing line reflect interactions between air masses of contrasting humidity (Galewsky and Samuels-Crow, 2015), and points below the Rayleigh curve typically signify local evaporation, such as from rain or open water (Worden et al., 2007). To specifically diagnose kinetic effects, we also examine a *q*–d-excess diagram (Fig. 6b), accounting for realistic polar conditions with Rayleigh curves modified for ice supersaturation ($RH_i$ = 100–110 %). Under these conditions, kinetic fractionation suppresses d-excess below equilibrium predictions (Jouzel and Merlivat, 1984; Jensen

https://doi.org/10.5194/egusphere-2025-5306
Preprint. Discussion started: 3 December 2025


and Pfister, 2005). Within this framework, points falling below the equilibrium curve primarily reflect d-excess suppression by ice-supersaturated cloud formation, whereas points above it indicate contributions from evaporation or sublimation (Samuels-Crow et al., 2014; Kopec et al., 2019). Collectively, these dual diagrams allow us to quantitatively distinguish the roles of long-range Rayleigh distillation, air-mass mixing, ice-phase microphysics, and local evaporation in shaping Arctic vapor isotopes across the sea ice regimes.

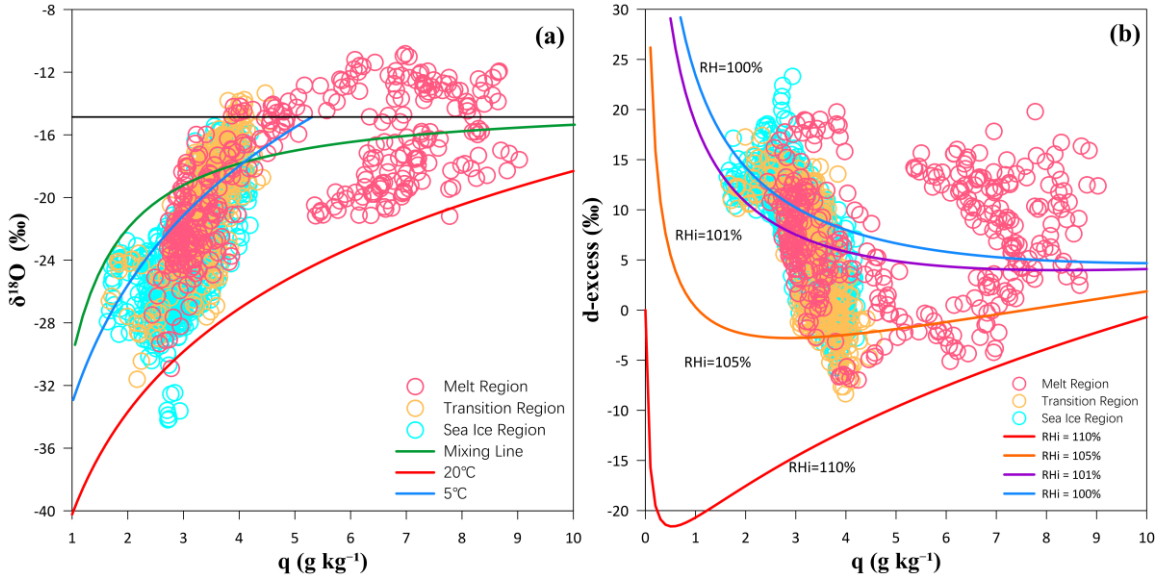


**Figure 6. Water vapor $\delta^{18}O$ (a) and d-excess (b) versus specific humidity ($q$). Data points are color-coded by sea ice regime. Theoretical Rayleigh distillation curves and mixing/supersaturation curves are shown in colored solid lines (see legends). The idealized Rayleigh curve shown in the graph was calculated based on an initial d-excess of 5.01‰ and $\delta^{18}O$ of –14.86‰ (the observed mean at 40–60°N). The initial specific humidity is 14.3 g kg$^{-1}$, corresponding to saturation over a 20°C surface water source (similar to the condition over 40–60°N open sea).**

In the Sea Ice and Transition Regions, $q$–$\delta^{18}O$ observations cluster near or between the 5 °C and 20 °C Rayleigh curves (Fig. 6a), consistent with vapor originating from advection and progressive dehydration during long-range transport. The $q$–d-excess relationship in these regions follows the Rayleigh equilibrium pattern (Fig. 6b), supporting the interpretation that Rayleigh distillation, rather than local kinetic fractionation, primarily governs water vapor isotopic variation in these regions. This also explains the contrasting temperature correlations observed in Fig. 4: a positive correlation for $\delta^{18}O$ but a negative one for d-excess, reflecting the advection of warm, humid air from lower-latitude oceanic regions toward the Arctic.

However, the decline in d-excess is steeper than predicted by the equilibrium Rayleigh curve, with many points falling below it (Fig. 6b). This deviation indicates additional kinetic fractionation, most likely from cloud formation under ice-supersaturated conditions, where the higher diffusivity of HDO compared to $H_2{}^{16}O$ leads to stronger fractionation of deuterium, suppressing d-excess (Clark and Fritz, 2013; Jouzel and Merlivat, 1984). Our calculations show that RH with respect to ice ($RH_i$) exceeding 105 %—common in polar regions—can reduce d-excess by over 10 ‰. Conversely, a limited number of points above the Rayleigh curve likely reflect contributions from sublimation of snow or sea ice (Kopec et al., 2019). Overall, the isotopic

https://doi.org/10.5194/egusphere-2025-5306
Preprint. Discussion started: 3 December 2025


composition of water vapor in the Sea Ice and Transition Regions is primarily governed by Rayleigh fractionation during advective transport, while d-excess provides a distinct, sensitive record of local kinetic processes at the ice-atmosphere interface, such as supersaturation and sublimation.

In contrast, the melt region exhibits a breakdown of the organized Rayleigh behaviour. Observations show a broad scatter in both $q$-$\delta^{18}O$ and $q$-d-excess diagrams, indicating the interplay between advected and locally evaporated vapor under ice-free conditions. At lower specific humidity (< 5 g/kg), isotopic patterns resemble those of ice-covered regions (Fig. 6), suggesting a persistent influence of advective moisture. However, as humidity rises (> 5 g/kg)—which coincides with surface air temperatures exceeding ~5 °C—systematic deviations from Rayleigh behavior become evident, reflecting the growing dominance of local processes. In the $q$–$\delta^{18}O$ diagram, two distinct patterns emerge: one cluster is enriched well above the mean mid-latitude $\delta^{18}O$ value, indicating input from warm, isotopically heavy sources; the other falls below the 5°C Rayleigh curve, where its scattered, non-logarithmic distribution—though still bounded by the 20°C curve and the mixing line—points to strong kinetic fractionation. This divergence is systematically mirrored in the $q$–d-excess diagram (Fig. 6b), where values split both below and above the equilibrium curve. The co-occurrence of $\delta^{18}O$ enrichment and elevated d-excess in this high-humidity regime directly implicates kinetic fractionation during local evaporation as an important driver of Arctic water vapor isotopic composition under ice-free conditions.

In summary, the isotopic composition of Arctic water vapor is governed by distinct processes that shift with the state of sea ice. In the Sea Ice and Transition Regions, isotope variations primarily reflect long-range Rayleigh distillation, partly modulated by kinetic effects from ice-phase processes such as supersaturation and sublimation. In the Melt Region, however, this regime gives way to a fundamentally different balance, in which local evaporation over open water emerges as the key control. Together, these results highlight that the state of sea ice fundamentally shapes the balance between advective and local processes governing Arctic water vapor isotopes.

### 3.4 Evaluating the Influence of Local Evaporation on Melt-Region Water Vapor Isotopes

To further evaluate the anomalous isotopic behavior identified with high temperature and humidity—where d-excess shows marked deviations from Rayleigh expectations under high-humidity conditions—we employed the MJ79 marine boundary-layer evaporation model (Merlivat and Jouzel, 1979; Bonne et al., 2019). The model was driven by observed surface temperature and relative humidity and accounts for both equilibrium fractionation, controlled by temperature, and kinetic fractionation, modulated by relative humidity. Following Bonne et al. (2019), we adopted kinetic fractionation factors representative of the rough-wind regime (>7 m $s^{-1}$) for all simulations.

https://doi.org/10.5194/egusphere-2025-5306
Preprint. Discussion started: 3 December 2025


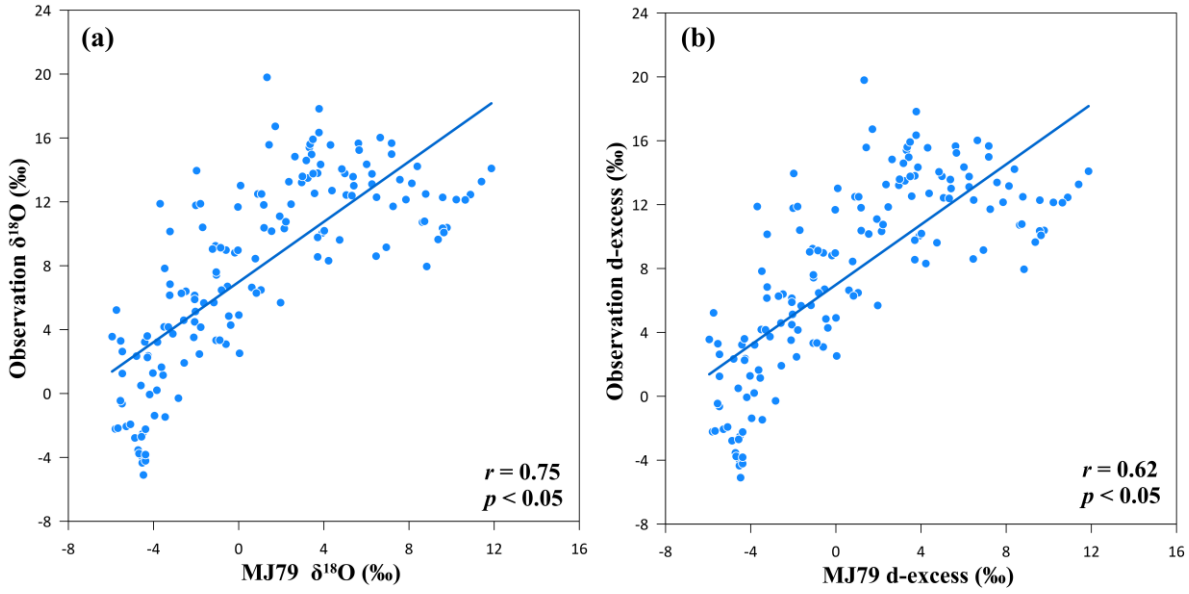


**Figure 7. Observed versus MJ79-simulated (a) $\delta^{18}O$ and (b) d-excess in the melt region for temperatures >5°C.**

Simulations were restricted to samples with temperatures exceeding 5 °C, corresponding to ice-free, high-humidity conditions where local evaporation is expected to dominate. Under these settings, the model reproduces the observed isotopic variability reasonably well, with correlations of 0.62 for $\delta^{18}O$ and 0.75 for d-excess (Fig. 7). This agreement supports the interpretation that kinetic fractionation during local evaporation contributes substantially to the isotopic composition of Arctic water vapor in the Melt Region. Nevertheless, since the observed vapor may also contain advected or recycled moisture, the actual contribution of local evaporation is likely smaller than the model estimate.

### 3.5 Moisture Source Attribution from Lagrangian Trajectory Analysis

To test our isotope-based interpretation of moisture sources, we computed 5-day backward trajectories from the cruise track using the HYSPLIT model, initialized every hour from 10 m altitude (Fig. 8). The analysis reveals a clear dichotomy in air mass origins aligned with sea ice regime. In the Sea Ice and Transition Regions, trajectories show air masses undergoing rapid cooling and dehydration during poleward transport, as reflected by declining specific humidity and rising relative humidity. Under these cold, saturated conditions, evaporation is suppressed, allowing Rayleigh distillation of advected moisture to emerge as the characteristic process, consistent with the observed alignment to Rayleigh curves (Fig. 6). Moreover, the frequent recirculation within the Arctic interior points to prolonged moisture residence under stable, cold conditions. This extended residency favors non-equilibrium ice-phase processes, such as supersaturation and sublimation, providing a coherent explanation for the distinctive *d*-excess signals observed in these regions (Fig. 6b).

In the Melt Region, however, trajectories reveal two distinct source pathways, explaining its complex isotopic signals. Most originate from lower latitudes, carrying warm, dry air northward across the Barents Sea. Elevated temperatures in the Barents

https://doi.org/10.5194/egusphere-2025-5306
Preprint. Discussion started: 3 December 2025


Sea create a large saturation vapor deficit (via the Clausius–Clapeyron relationship), which maintains low relative humidity despite high specific humidity. These conditions promote strong evaporation over the ice-free ocean, contributing to the d-excess enrichment observed in this region (Fig. 4) and confirming that local evaporation is a major driver of isotopic variability under melt conditions. A smaller subset of air masses recirculates within the cold, saturated Arctic interior. Their limited interaction with open water suppresses evaporation, preserving an advective signature similar to that of ice-covered regions. Together, these dual air mass origins—one characterized by strong local evaporation and the other by advected moisture—explain the coexistence of both isotopic end-members observed in the $q$–$\delta^{18}O$ and $q$–d-excess relationships.

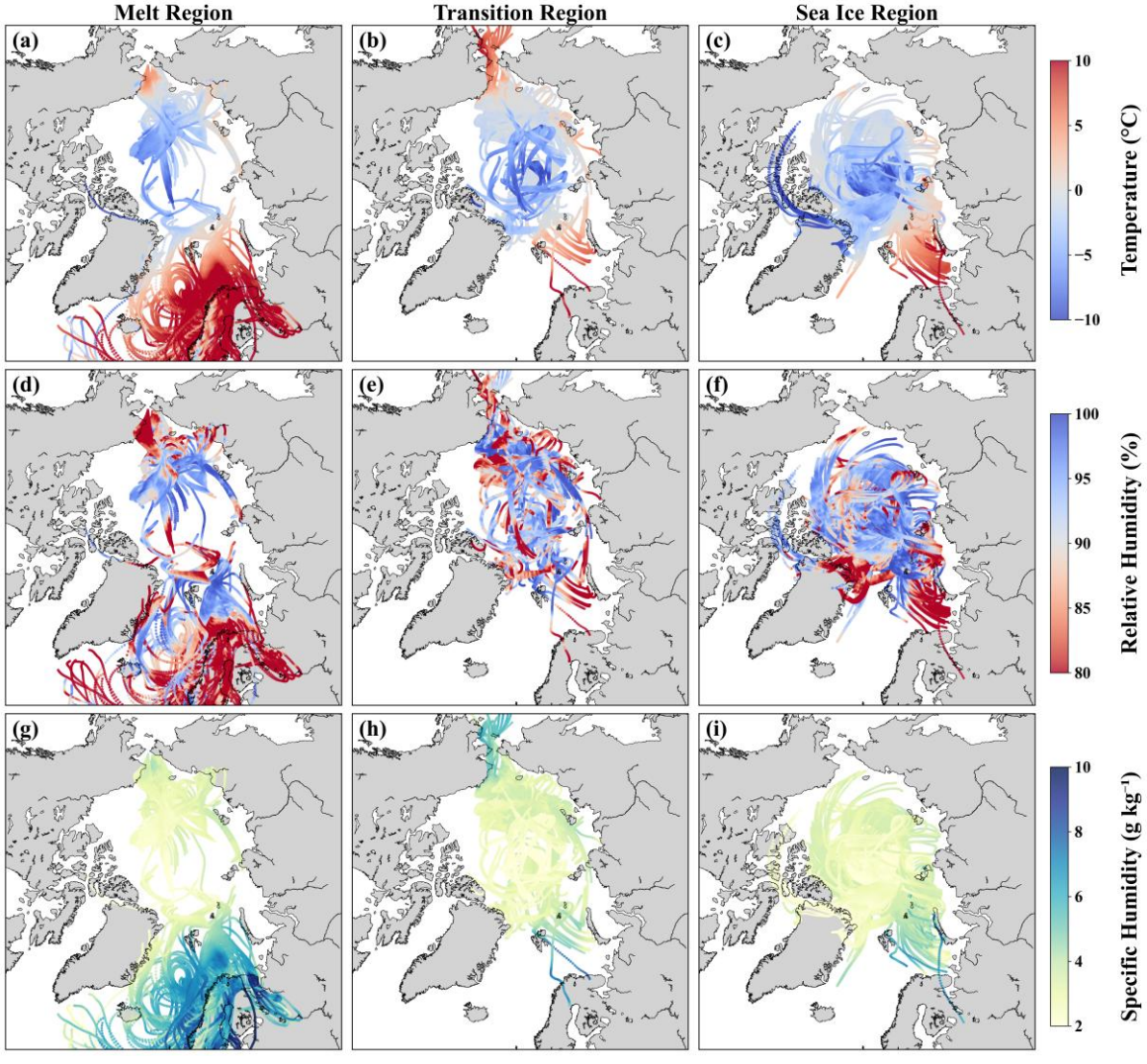


**Figure 8. Five-day HYSPLIT backward trajectories and associated meteorological variables, grouped by sea ice regime. Columns represent the melt (left), transition (middle), and sea ice (right) regions; rows show air temperature (a–c, °C), relative humidity (d–f, %), and specific humidity (g–i, g kg$^{-1}$). Trajectories were computed hourly along the cruise track, illustrating the air mass evolution prior to sampling.**

https://doi.org/10.5194/egusphere-2025-5306
Preprint. Discussion started: 3 December 2025


### 3.6 Relative Contributions of Moisture Sources Across Arctic Sea Ice Regimes

To quantify the relative contributions of locally evaporated and advected moisture to Arctic boundary layer water vapor across different sea ice regimes, we apply the Bayesian isotope mixing model MixSIAR (Stock et al., 2018) to $\delta^{18}O$ and $\delta D$ measurements. Locally evaporated moisture is derived from Arctic open-water evaporation, with $\delta^{18}O = -11.77 \pm 0.59$ ‰ and $\delta D = -96.02 \pm 7.67$ ‰, estimated using the MJ79 model (Methods). Advected lower-latitude moisture, as identified by HYSPLIT trajectories (Fig. 8), primarily originates from the North Atlantic and the North Pacific, with isotopic endmembers taken from Benetti et al. (2017) near 55°N for the Atlantic ($\delta^{18}O = -18.25 \pm 2.07$ ‰, $\delta D = -138.53 \pm 34.75$ ‰) and from our observations over 40–60°N for the Pacific ($\delta^{18}O = -14.86 \pm 2.07$ ‰, $\delta D = -113.87 \pm 15.44$ ‰). A weighted average based on trajectory counts (83.8 % Atlantic, 16.2 % Pacific) is used to represent a single lower-latitude source ($\delta^{18}O = -17.49 \pm 4.79$ ‰, $\delta D = -134.53 \pm 34.2$ ‰). Measured and calibrated vapor isotope values from each sea ice regime serve as the mixture input. A process error structure is applied to account for spatial variability and source uncertainty (Methods), and MixSIAR is run independently for each regime to estimate the probability distributions of source contributions.

MixSIAR results reveal a clear spatial gradient in moisture source contributions across sea ice regimes (Fig. 9). Local evaporation contributes most in the Melt Region, with a mean of 22.7 % (95 % CI: 1.2–50.4 %), decreasing to 15.2 % (95 % CI: 0.6–39.4 %) in the Transition Region and 9.3 % (95 % CI: 0.3–27.1 %) in the Sea Ice Region. Although the absolute contribution of local evaporation is modest, it increases progressively with decreasing sea ice cover. Across all regimes, advected lower-latitude moisture remains the dominant source, accounting for 77–91 % of boundary-layer vapor. These findings indicate that, while long-range transport governs the Arctic vapor budget, local evaporation contributes a notable fraction in ice-free areas.

https://doi.org/10.5194/egusphere-2025-5306
Preprint. Discussion started: 3 December 2025


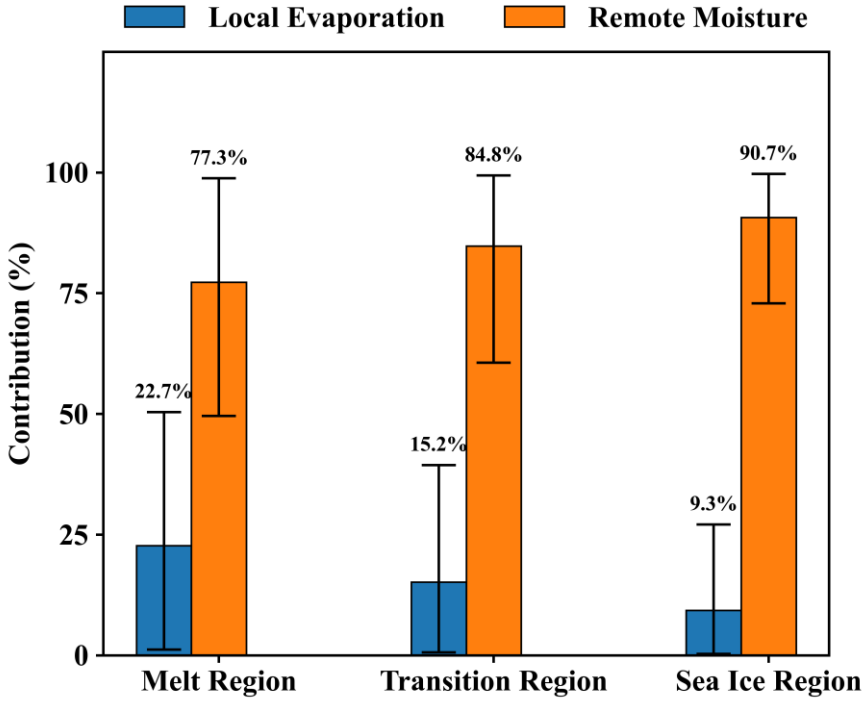


**Figure 9. Contributions of local and low-latitude remote moisture estimated using a Bayesian isotope mixing model. Blue and orange bars indicate the proportions of local and low-latitude sources, respectively. Error bars denote the 95% credible intervals (2.5–97.5%), and the values above each bar represent the mean contributions.**

## 4 Discussion and Conclusions

This study demonstrates that Arctic near-surface water vapor isotopes are systematically regulated by sea ice regimes, which control moisture sources and fractionation pathways. Under extensive ice, advective Rayleigh distillation dominates, producing a strong $\delta^{18}O$–temperature correlation and elevated d-excess in colder regions. As sea ice retreats, local evaporation over open water contributes more, imprinting a kinetic fingerprint of enriched $\delta^{18}O$ and elevated d-excess under warm, dry conditions. This shift breaks down the canonical $\delta^{18}O$–temperature relationship, giving rise to an "anti-temperature" effect. Quantifying this regime shift, our Bayesian mixing model constrained by in-situ isotopes reveals that local evaporation contributions rise from 9.3% in the Sea Ice Region to 22.7% in the Melt Region—demonstrating a 2.4-fold enhancement of local recycling despite persistent advective dominance. These results establish sea ice as the dynamic regulator of Arctic isotopic variability across the ice–open water transition, offering direct observational benchmarks that constrain both contemporary hydroclimate changes and paleoclimate reconstructions.

Our sea-ice–based isotope framework resolves a longstanding Arctic paradox by showing that, although d-excess has traditionally been treated predominantly as a source signature (Dansgaard, 1964), it is highly sensitive to boundary-layer thermodynamics governed by sea-ice extent. Since the first polar vapor isotope measurements reported unexpectedly higher

https://doi.org/10.5194/egusphere-2025-5306
Preprint. Discussion started: 3 December 2025


d-excess in Arctic-sourced moisture compared with lower latitudes (Kurita, 2011), subsequent studies have alternately documented both high (Kopec et al., 2019; Pang et al., 2019) and low (Samuels-Crow et al., 2014; Klein et al., 2015; Klein and Welker, 2016; Brunello et al., 2023) values under similar surface conditions. These apparently conflicting results reflect sampling across a continuum of ice-controlled humidity and kinetic fractionation regimes rather than intrinsic differences in moisture sources. Cold, near-saturated ice-covered conditions suppress kinetic effects, producing higher d-excess driven by equilibrium processes, whereas warm, dry open-water conditions enhance kinetic evaporation, elevating d-excess and generating the characteristic anti-temperature $\delta^{18}O$ signal. By explicitly accounting for these sea-ice state-dependent controls, our work reconciles these observations and provides a physically consistent basis for interpreting Arctic vapor isotopes.

Quantification of moisture source contributions across sea ice regimes further elucidates the broader implications of this continuum. Local evaporation rises from 9.3 % in the Sea Ice Region to 22.7 % in the Melt Region, demonstrating enhanced local recycling despite persistent advective dominance. This gradient aligns with observed surface moisture flux trends (Boisvert and Stroeve, 2015) and contextualizes previous observationally or model-based estimates ranging from 8 % (Domínguez et al., 2018) to over 35 % (Zhong et al., 2018). Differences among studies likely reflect variations in seasonal and spatial sampling, methodological choices, and isotopic assumptions, including simplified treatment of evaporation in the MJ79 model and limited constraints on low-latitude endmembers. Crucially, these results demonstrate that local contributions are intrinsically tied to sea-ice state, quantifying a previously hypothesized feedback whereby sea ice retreat promotes a more localized water cycle, as recorded in Arctic water vapor (Bailey et al., 2021) and precipitation (Kopec et al., 2016) isotopes. These observations provide the first in-situ isotopic benchmark for evaluating near-surface humidity, precipitation recycling, and the fidelity of regional climate models.

Beyond contemporary implications, our findings necessitate refinements in paleoclimate interpretations from polar ice-core records. The canonical $\delta^{18}O$–temperature relationship, long used as a paleo-thermometer, is modulated by sea ice extent: under extensive ice cover, strong positive correlations reflect temperature-driven advective distillation, whereas in Transition and Melt Regions, the relationship weakens or reverses (“anti-temperature” effect), indicating that $\delta^{18}O$ integrates local evaporation and humidity signals alongside temperature. Enriched $\delta^{18}O$ with elevated d-excess during warm, ice-reduced periods (e.g., interglacials) reflects reorganized local moisture sources rather than temperature alone. We advocate a regime-informed dual-proxy framework that leverages $\delta^{18}O$–d-excess co-variation, interpreted through modern-observed sea ice regimes, to disentangle past temperature and sea ice signals—thereby reconciling observational contradictions and bridging modern process understanding with paleo-isotope interpretation.

While our study establishes a sea ice–mediated isotopic framework, several research frontiers warrant further investigation. Extending observations across seasons and years will test the climatological robustness of the framework, while expanding spatial coverage and incorporating additional tracers (e.g., $^{17}O$-excess) will refine mechanistic attribution. Integrating the framework into isotope-enabled climate models can evaluate model performance across both past and projected climates, and applying it to ice-core records will help disentangle temperature and sea ice signals. Collectively, these efforts will advance

https://doi.org/10.5194/egusphere-2025-5306
Preprint. Discussion started: 3 December 2025


Arctic isotope science from descriptive regime characterization to predictive understanding of hydroclimate responses under accelerating global change.

## Data and code availability

The ERA5 data are publicly available at: https://cds.climate.copernicus.eu/datasets (last access : September 2025). The SIC data were adopted from the National Snow and Ice Data Center (NSIDC) at: https://nsidc.org/data/g10005/versions/2 (last access : September 2025). The Global Data Assimilation System (GDAS) meteorological fields were obtained from NOAA's Air Resources Laboratory (ftp://arlftp.arlhq.noaa.gov/pub/archives/gdas1/ (last access : September 2025)). The water vapor isotope dataset and the code to reproduce the figures in the main text will be available on the Zenodo research data repository after manuscript publication.

## Author contributions

Yuankun Zhang and Zhongfang Liu designed the research. Yuankun Zhang, Dongsheng Li, Zhiqing Li and Hebin Shao performed the investigation, including the deployment and calibration of the ship-based instruments. Yuankun Zhang, Zhongfang Liu, and Dongsheng Li performed the analysis. All authors contributed to the discussion of the results and the final article. Yuankun Zhang drafted the paper with contributions from all co-authors. Zhongfang Liu checked and modified the paper.

## Competing interests

The authors declare that they have no conflict of interest.

## Acknowledgments

We gratefully acknowledge the open-source contributions of Stock and Semmens for the MixSIAR R package, NOAA for the HYSPLIT model, and Daniel Warner for the development and sharing of the pysplit package. Furthermore, we extend our sincere gratitude to all members of the 14th Chinese National Arctic Research Expedition, especially the crew and scientists aboard the RV *Xuelong 2*, for providing an exceptional operational environment and foundational support for the measurements conducted in this study.

## Financial support

https://doi.org/10.5194/egusphere-2025-5306
Preprint. Discussion started: 3 December 2025


This work is supported by the National Natural Science Foundation of China (Grant 42025602).

## References

Bailey, H., Hubbard, A., Klein, E. S., Mustonen, K. R., Akers, P. D., Marttila, H., and Welker, J. M.: Arctic sea-ice loss fuels extreme European snowfall, Nat. Geosci., 14, 283-288, https://doi.org/10.1038/s41561-021-00719-y, 2021.

Barras, V. and Simmonds, I.: Observation and modeling of stable water isotopes as diagnostics of rainfall dynamics over southeastern Australia, Journal of Geophysical Research-Atmospheres, 114, 17, https://doi.org/10.1029/2009jd012132, 2009.

Benetti, M., Steen-Larsen, H. C., Reverdin, G., Sveinbjornsdottir, A. E., Aloisi, G., Berkelhammer, M. B., Bourles, B., Bourras, D., De Coetlogon, G., Cosgrove, A., Faber, A. K., Grelet, J., Hansen, S. B., Johnson, R., Legoff, H., Martin, N., Peters, A. J., Popp, T. J., Reynaud, T., and Winther, M.: Stable isotopes in the atmospheric marine boundary layer water vapour over the Atlantic Ocean, 2012-2015, Sci. Data, 4, 17, https://doi.org/10.1038/sdata.2016.128, 2017.

Bengtsson, L., Hodges, K. I., Koumoutsaris, S., Zahn, M., and Keenlyside, N.: The changing atmospheric water cycle in Polar Regions in a warmer climate, Tellus Ser. A-Dyn. Meteorol. Oceanol., 63, 907-920, https://doi.org/10.1111/j.1600-0870.2011.00534.x, 2011.

Bintanja, R. and Selten, F. M.: Future increases in Arctic precipitation linked to local evaporation and sea-ice retreat, Nature, 509, 479-482, https://doi.org/10.1038/nature13259, 2014.

Boisvert, L. N. and Stroeve, J. C.: The Arctic is becoming warmer and wetter as revealed by the Atmospheric Infrared Sounder, Geophys. Res. Lett., 42, 4439-4446, https://doi.org/10.1002/2015gl063775, 2015.

Bonne, J. L., Behrens, M., Meyer, H., Kipfstuhl, S., Rabe, B., Schönicke, L., Steen-Larsen, H. C., and Werner, M.: Resolving the controls of water vapour isotopes in the Atlantic sector, Nat. Commun., 10, 1632, https://doi.org/10.1038/s41467-019-09242-6, 2019.

Bowen, G. J., Cai, Z. Y., Fiorella, R. P., and Putman, A. L.: Isotopes in the water cycle: regional- to global-scale patterns and applications, in: Annual review of earth and planetary sciences, Vol 47, Annual Review of Earth and Planetary Sciences, edited by: Jeanloz, R., and Freeman, K. H., Annual Reviews, Palo Alto, 453-479, https://doi.org/10.1146/annurev-earth-053018-060220, 2019.

Brunello, C. F., Meyer, H., Mellat, M., Casado, M., Bucci, S., Dütsch, M., and Werner, M.: Contrasting seasonal isotopic signatures of near-surface atmospheric water vapor in the central Arctic during the MOSAiC campaign, Journal of Geophysical Research-Atmospheres, 128, e2022JD038400, https://doi.org/10.1029/2022jd038400, 2023.

Clark, I. D. and Fritz, P.: Environmental isotopes in hydrogeology, CRC press, ISBN 042906957X, 2013

Dansgaard, W.: Stable isotopes in precipitation, Tellus, 16, 436-468, https://doi.org/10.3402/tellusa.v16i4.8993, 1964.

Domínguez, M. V., Muñiz, R. N., Drumond, A., and Presa, L. G.: Moisture transport from the Arctic: A characterization from a Lagrangian perspective, Cuadernos de investigación geográfica: Geographical Research Letters, 44, 659-673, https://doi.org/10.18172/cig.3477, 2018.

Fetterer, F., Stewart, J. S., and Meier, W. N.: MASAM2: Daily 4 km Arctic sea ice concentration (Version 2), National Snow and Ice Data Center [dataset],https://doi.org/10.7265/bqd9-vm28, 2023.

Ford, V. L. and Frauenfeld, O. W.: Arctic precipitation recycling and hydrologic budget changes in response to sea ice loss, Glob. Planet. Change, 209, 103752, https://doi.org/10.1016/j.gloplacha.2022.103752, 2022.

Galewsky, J. and Samuels-Crow, K.: Summertime moisture transport to the southern south American Altiplano: constraints from in situ measurements of water vapor isotopic composition, J. Clim., 28, 2635-2649, https://doi.org/10.1175/jcli-d-14-00511.1, 2015.

Galewsky, J., Steen-Larsen, H. C., Field, R. D., Worden, J., Risi, C., and Schneider, M.: Stable isotopes in atmospheric water vapor and applications to the hydrologic cycle, Rev. Geophys., 54, 809-865, https://doi.org/10.1002/2015rg000512, 2016.

Gao, J., Masson-Delmotte, V., Yao, T., Tian, L., Risi, C., and Hoffmann, G.: Precipitation Water Stable Isotopes in the South Tibetan Plateau: Observations and Modeling, J. Clim., 24, 3161-3178, https://doi.org/10.1175/2010jcli3736.1, 2011.

Gat, J. R.: Oxygen and hydrogen isotopes in the hydrologic cycle, Annu. Rev. Earth Planet. Sci., 24, 225-262, https://doi.org/10.1146/annurev.earth.24.1.225, 1996.

https://doi.org/10.5194/egusphere-2025-5306
Preprint. Discussion started: 3 December 2025


Gimeno, L., Eiras-Barca, J., Durán-Quesada, A. M., Dominguez, F., van der Ent, R., Sodemann, H., Sánchez-Murillo, R., Nieto, R., and Kirchner, J. W.: The residence time of water vapour in the atmosphere, Nat. Rev. Earth Environ., 2, 558-569, https://doi.org/10.1038/s43017-021-00181-9, 2021.
Graversen, R. G., Mauritsen, T., Tjernström, M., Källén, E., and Svensson, G.: Vertical structure of recent Arctic warming, Nature, 451, 53-U54, https://doi.org/10.1038/nature06502, 2008.
Hersbach, H., Comyn-Platt, E., Bell, B., Berrisford, P., Biavati, G., Horányi, A., Sabater, J. M., Nicolas, J., Peubey, C., and Radu, R.: ERA5 post-processed daily-statistics on pressure levels from 1940 to present. Copernicus Climate Change Service (C3S) Climate Data Store (CDS), 10.24381/cds.4991cf48, 2023.
Jensen, E. and Pfister, L.: Implications of persistent ice supersaturation in cold cirrus for stratospheric water vapor, Geophys. Res. Lett., 32, L01808, https://doi.org/10.1029/2004gl021125, 2005.
Jouzel, J. and Merlivat, L.: Deuterium and O-18 in precipitation - modeling of the isotopic effects during snow formation, Journal of Geophysical Research-Atmospheres, 89, 1749-1757, https://doi.org/10.1029/JD089iD07p11749, 1984.
Klein, E. S. and Welker, J. M.: Influence of sea ice on ocean water vapor isotopes and Greenland ice core records, Geophys. Res. Lett., 43, 12475-12483, https://doi.org/10.1002/2016gl071748, 2016.
Klein, E. S., Cherry, J. E., Young, J., Noone, D., Leffler, A. J., and Welker, J. M.: Arctic cyclone water vapor isotopes support past sea ice retreat recorded in Greenland ice, Sci Rep, 5, 10295, https://doi.org/10.1038/srep10295, 2015.
Klein, E. S., Nolan, M., McConnell, J., Sigl, M., Cherry, J., Young, J., and Welker, J. M.: McCall Glacier record of Arctic climate change: Interpreting a northern Alaska ice core with regional water isotopes, Quat. Sci. Rev., 131, 274-284, https://doi.org/10.1016/j.quascirev.2015.07.030, 2016.
Kopec, B. G., Feng, X., Posmentier, E. S., and Sonder, L. J.: Seasonal Deuterium Excess Variations of Precipitation at Summit, Greenland, and their Climatological Significance, Journal of Geophysical Research-Atmospheres, 124, 72-91, https://doi.org/10.1029/2018jd028750, 2019.
Kopec, B. G., Feng, X. H., Michel, F. A., and Posmentier, E. S.: Influence of sea ice on Arctic precipitation, Proc. Natl. Acad. Sci. U. S. A., 113, 46-51, https://doi.org/10.1073/pnas.1504633113, 2016.
Kurita, N.: Origin of Arctic water vapor during the ice-growth season, Geophys. Res. Lett., 38, L02709, https://doi.org/10.1029/2010gl046064, 2011.
Liu, J. F., Xiao, C. D., Ding, M. H., and Ren, J. W.: Variations in stable hydrogen and oxygen isotopes in atmospheric water vapor in the marine boundary layer across a wide latitude range, J. Environ. Sci., 26, 2266-2276, https://doi.org/10.1016/j.jes.2014.09.007, 2014.
Mellat, M., Bailey, H., Mustonen, K. R., Marttila, H., Klein, E. S., Gribanov, K., Bret-Harte, M. S., Chupakov, A. V., Divine, D. V., Else, B., Filippov, I., Hyöky, V., Jones, S., Kirpotin, S. N., Kroon, A., Markussen, H. T., Nielsen, M., Olsen, M., Paavola, R., Pokrovsky, O. S., Prokushkin, A., Rasch, M., Raundrup, K., Suominen, O., Syvänperä, I., Vignisson, S. R., Zarov, E., and Welker, J. M.: Hydroclimatic controls on the isotopic ($\delta^{18}O$, $\delta^{2}H$, d-excess) traits of Pan-Arctic summer rainfall events, Front. Earth Sci., 9, 651731, https://doi.org/10.3389/feart.2021.651731, 2021.
Merlivat, L. and Jouzel, J.: Global climatic interpretation of the deuterium-oxygen-18 relationship for precipitation, J. Geophys. Res.-Oceans, 84, 5029-5033, https://doi.org/10.1029/JC084iC08p05029, 1979.
Min, S. K., Zhang, X. B., and Zwiers, F.: Human-induced arctic moistening, Science, 320, 518-520, https://doi.org/10.1126/science.1153468, 2008.
Namyatov, A. A., Tokarev, I. V., and Pastukhov, I. A.: Results of the Barents Sea waters isotopic studies. R/V "Dalnie Zelentsy" March-April 2021 (V1), Mendeley Data [dataset],https://doi.org/10.17632/nvkf2f8xdd.1, 2023.
Namyatov, A. A., Tokarev, I. V., and Pastukhov, I. A.: Genesis of the eastern Barents Sea part water masses using winter data of isotopic parameters $\delta^{18}O$ and $\delta^{2}H$, Deep-Sea Res. Part I-Oceanogr. Res. Pap., 208, 104302, https://doi.org/10.1016/j.dsr.2024.104302, 2024.
Noone, D.: Pairing measurements of the water vapor isotope ratio with humidity to deduce atmospheric moistening and dehydration in the tropical midtroposphere, J. Clim., 25, 4476-4494, https://doi.org/10.1175/jcli-d-11-00582.1, 2012.
Opel, T., Fritzsche, D., and Meyer, H.: Eurasian Arctic climate over the past millennium as recorded in the Akademii Nauk ice core (Severnaya Zemlya), Clim. Past., 9, 2379-2389, https://doi.org/10.5194/cp-9-2379-2013, 2013.
Pang, H. X., Hou, S. G., Landais, A., Masson-Delmotte, V., Jouzel, J., Steen-Larsen, H. C., Risi, C., Zhang, W. B., Wu, S. Y., Li, Y. S., An, C. L., Wang, Y. T., Prie, F., Minster, B., Falourd, S., Stenni, B., Scarchilli, C., Fujita, K., and Grigioni, P.: Influence of summer sublimation on δD, $\delta^{18}O$, and $\delta^{17}O$ in precipitation, east Antarctica, and implications for climate

https://doi.org/10.5194/egusphere-2025-5306
Preprint. Discussion started: 3 December 2025


reconstruction from ice cores, Journal of Geophysical Research-Atmospheres, 124, 7339-7358, https://doi.org/10.1029/2018jd030218, 2019.
Porter, S. E., Mosley-Thompson, E., and Thompson, L. G.: Ice Core δ18O Record Linked to Western Arctic Sea Ice Variability, Journal of Geophysical Research-Atmospheres, 124, 10784-10801, https://doi.org/10.1029/2019jd031023, 2019.
Samuels-Crow, K. E., Galewsky, J., Sharp, Z. D., and Dennis, K. J.: Deuterium excess in subtropical free troposphere water vapor: Continuous measurements from the Chajnantor Plateau, northern Chile, Geophys. Res. Lett., 41, 8652-8659, https://doi.org/10.1002/2014gl062302, 2014.
Screen, J. A., Deser, C., and Simmonds, I.: Local and remote controls on observed Arctic warming, Geophys. Res. Lett., 39, L10709, https://doi.org/10.1029/2012gl051598, 2012.
Shao, L. L., Tian, L. D., Cai, Z. Y., Wang, C., and Li, Y.: Large-scale atmospheric circulation influences the ice core d-excess record from the central Tibetan Plateau, Clim. Dyn., 57, 1805-1816, https://doi.org/10.1007/s00382-021-05779-9, 2021.
Song, W. X., Liu, Z. F., Lan, H. M., and Huan, X. H.: Influence of seasonal sea-ice loss on Arctic precipitation δ18O: a GCM-based analysis of monthly data, Polar Res., 42, 1-13, https://doi.org/10.33265/polar.v42.9751, 2023.
Steen-Larsen, H. C., Johnsen, S. J., Masson-Delmotte, V., Stenni, B., Risi, C., Sodemann, H., Balslev-Clausen, D., Blunier, T., Dahl-Jensen, D., Ellehoj, M. D., Falourd, S., Grindsted, A., Gkinis, V., Jouzel, J., Popp, T., Sheldon, S., Simonsen, S. B., Sjolte, J., Steffensen, J. P., Sperlich, P., Sveinbjörnsdóttir, A. E., Vinther, B. M., and White, J. W. C.: Continuous monitoring of summer surface water vapor isotopic composition above the Greenland Ice Sheet, Atmos. Chem. Phys., 13, 4815-4828, https://doi.org/10.5194/acp-13-4815-2013, 2013.
Stein, A. F., Draxler, R. R., Rolph, G. D., Stunder, B. J. B., Cohen, M. D., and Ngan, F.: NOAA'S HYSPLIT atmospheric transport and dispersion modeling system, Bull. Amer. Meteorol. Soc., 96, 2059-2077, https://doi.org/10.1175/bams-d-14-00110.1, 2015.
Stock, B. and Semmens, B.: MixSIAR GUI user manual v3. 1,https://doi.org/10.5281/zenodo.1209993, 2016a.
Stock, B. C. and Semmens, B. X.: Unifying error structures in commonly used biotracer mixing models, Ecology, 97, 2562-2569, https://doi.org/10.1002/ecy.1517, 2016b.
Stock, B. C., Jackson, A. L., Ward, E. J., Parnell, A. C., Phillips, D. L., and Semmens, B. X.: Analyzing mixing systems using a new generation of Bayesian tracer mixing models, PeerJ, 6, e5096, https://doi.org/10.7717/peerj.5096, 2018.
Sturm, C., Zhang, Q., and Noone, D.: An introduction to stable water isotopes in climate models: benefits of forward proxy modelling for paleoclimatology, Clim. Past., 6, 115-129, https://doi.org/10.5194/cp-6-115-2010, 2010.
Uemura, R., Matsui, Y., Yoshimura, K., Motoyama, H., and Yoshida, N.: Evidence of deuterium excess in water vapor as an indicator of ocean surface conditions, Journal of Geophysical Research-Atmospheres, 113, D19114, https://doi.org/10.1029/2008jd010209, 2008.
Wallace, J. M. and Hobbs, P. V.: Atmospheric science: an introductory survey, Elsevier, ISBN 0080499538, 2006
Wang, D., Tian, L. D., Risi, C., Wang, X. J., Cui, J. P., Bowen, G. J., Yoshimura, K., Wei, Z. W., and Li, L. Z. X.: Vehicle-based in situ observations of the water vapor isotopic composition across China: spatial and seasonal distributions and controls, Atmos. Chem. Phys., 23, 3409-3433, https://doi.org/10.5194/acp-23-3409-2023, 2023.
Warner, M. S. C.: Introduction to PySPLIT: A Python toolkit for NOAA ARL's HYSPLIT model, Comput. Sci. Eng., 20, 47-62, https://doi.org/10.1109/mcse.2017.3301549, 2018.
Worden, J., Noone, D., Bowman, K., and Tropospheric Emission, S.: Importance of rain evaporation and continental convection in the tropical water cycle, Nature, 445, 528-532, https://doi.org/10.1038/nature05508, 2007.
Xi, X.: A review of water isotopes in atmospheric general circulation models: recent advances and future prospects, International Journal of Atmospheric Sciences, 2014, 250920, https://doi.org/10.1155/2014/250920, 2014.
Xiang, Q. Y., Liu, G. D., Meng, Y. C., Chen, K., and Xia, C. C.: Temporal trends of deuterium excess in global precipitation and their environmental controls under a changing climate, J. Radioanal. Nucl. Chem., 331, 3633-3649, https://doi.org/10.1007/s10967-022-08414-x, 2022.
Zhong, L. H., Hua, L. J., and Luo, D. H.: Local and external moisture sources for the Arctic warming over the Barents-Kara seas, J. Clim., 31, 1963-1982, https://doi.org/10.1175/jcli-d-17-0203.1, 2018.